Transfer of spin angular momentum of an incident wave into orbital angular momentum of the bound states in the continuum in an array of dielectric spheres

Evgeny N. Bulgakov[1,2] and Almas F. Sadreev[1]

[1]*Kirensky Institute of Physics, Federal Research Center KSC SB RAS, 660036 Krasnoyarsk, Russia*
[2]*Siberian State Aerospace University, Krasnoyarsk 660014, Russia*

We consider scattering of electromagnetic plane waves by a linear periodic array of dielectric spheres. For incident waves with circular polarization with frequency tuned to the bound states with orbital angular momentum in the radiation continuum, the spin angular momentum of the incident wave transfers into the orbital angular momentum. This, in turn, gives rise to giant vortical power currents rotating around the array. Incident wave with linear polarization with frequency tuned to the Bloch bound state in the continuum induces giant laminar power currents.

I. INTRODUCTION

It is well known that electromagnetic (EM) fields cannot only carry energy but also angular momentum. The angular momentum is composed of the spin angular momentum (SAM) and the orbital angular momentum (OAM) describing the polarization and the phase structure distribution of EM fields, respectively. The research on the OAM of EM fields has been of interest since Allen *et al.* investigated the mechanism of the OAM in laser modes [1,2]. In contrast to SAM, which has only two possible states of left-handed and right-handed circular polarizations, the states of OAM are in principle unlimited owing to the unique characteristics of spiral flow of propagating EM waves [3]. The OAM has the potential to tremendously increase the spectral efficiency and capacity of communication systems [4]. Among numerous investigations on OAM effects, one of the subjects of intensive recent studies is the link between the near-field chirality and the far-field OAM. For different types of chiral polaritonic lenses, it was shown that the near-field chirality can lead to the tailoring optical OAM in the far-field region [5,6]. There have been many proposals to generate OAM beams by use of chiral plasmonic nanostructures [5], ferrite particles [7], monolithic integration of spiral phase plates [8], chiral polaritonic lenzes [9], designer metasurfaces [10], *etc.*

Schäferling *et al.* [11] have shown that chiral fields, i.e., electromagnetic fields with nonvanishing optical chirality, can occur next to symmetric nanostructures without geometrical chirality illuminated with linearly polarized light at normal incidence. Rodriguez-Fortuño *et al.* [12] demonstrated a planar photonic nanostructure with no chirality consisting of a silicon microdisk coupled to two waveguides. The device distinguishes the handedness of an incoming circularly polarized light beam by driving photons with opposite spins toward different waveguides. It was shown theoretically and experimentally that the fundamental resonance of a silicon microdisk resonator can inherit the angular momentum carried by anormally incident light beam and transfer it as linear momentum into one of two output waveguides. Remarkably, the microdisk is not chiral: It responds equally to the left chiral polarization and the right chiral polarization without exhibiting optical activity or circular dichroism. Instead, it couples light to different waveguides (with opposite linear

momenta) depending on the handedness of incoming light and the relative position between the microdisk and the waveguides.

The above results have a simple interpretation by an analog with the spin-orbit interaction $\lambda \vec{S} \vec{L}$ in atomic spectroscopy where $\vec{S}$ is the SAM and $\vec{L} = \vec{r} \times \vec{p}$ is the OAM. The transfer of SAM to OAM is well known as a resonant transition between the electron bound state without OAM and the state with OAM. Our primary goal is to show a similar transfer of SAM to OAM of bound states in all-dielectric system. It has been widely believed that only those electromagnetic (EM) modes whose eigenfrequencies lie below the light cone are confined in dielectric systems and the rest of the eigenmodes have finite life times. Recently, confined EM modes, i.e., bound states in the radiation continuum (BSC) were shown to exist in various periodical arrays of (i) long cylindrical rods [13–18], (ii) photonic crystal slabs [19–24], (iii) two-dimensional arrays of spheres [25], (iv) core-shell single spheres [26–28], and (v) one-dimensional array of dielectric spheres [29]. The BSCs are of immense interest in optics because of the experimental opportunity to confine light despite the fact that outgoing waves are allowed in the surrounding medium.

The most simple symmetry-protected TE and TM polarized BSCs found in Ref. [29] have both zero OAM $m = 0$ and the Bloch vector $\beta_c = 0$ and occur in a wide range of the radii of the spheres and dielectric constants. Alongside Bloch BSCs with $\beta_c \neq 0$ and BSC with OAM $m \neq 0$ were shown to exist. The Bloch BSC is a traveling wave with a definite Bloch vector β_c directed along the array. These BSCs are degenerate with respect to the sgn of β_c. Although true BSCs are invisible in scattering of plane waves their effect can be substantial in the vicinity of the BSC point in the parametric space of the incident wave: frequency, wave vector, and polarization as well as material parameters of the spheres [15,29]. In particular a plane wave with the frequency and angle of incidence tuned close to the Bloch BSC point excites the Bloch BSC with giant currents flowing along the array. The BSCs have the important for optical applications property to enormously enhance the incident wave [25,30,31]. Thus the plane wave is capable of initiating giant laminar power currents in dielectric arrays.

BSCs with OAM are more interesting. Because of the axial symmetry of the array these BSCs are degenerate relative to

azimuthal number $\pm m$. Illumination by a plane wave with linear polarization equally excites both degenerate BSCs, resulting in currents with zero OAM (zero vorticity). The plane wave with circular polarization excites the BSCs with either $m > 0$ or $m < 0$ as dependent on the polarization. Therefore the plane wave with circular polarization induces a giant power current spinning around the array axis. In other words, plane wave with SAM transfers the spin angular momentum onto the orbital angular momentum with giant vortical power currents.

II. BASIC EQUATIONS FOR EM WAVE SCATTERING BY A LINEAR ARRAY OF SPHERES

In the present paper we consider a free-standing one-dimensional infinite array of dielectric spheres in air (Fig. 1). In what follows we refer to all length quantities in terms of the period h of the array.

We seek the solutions of the Maxwell equations, which obey the Bloch theorem

$$\mathbf{E}(\mathbf{r} + \mathbf{R}_j) = e^{i\beta \mathbf{R}_j}\mathbf{E}(\mathbf{r}), \quad \mathbf{H}(\mathbf{r} + \mathbf{R}_j) = e^{i\beta \mathbf{R}_j}\mathbf{H}(\mathbf{r}),$$

with the Bloch wave vector β directed along the array aligned with the z axis (see Fig. 1). Here $\mathbf{R}_j = j\mathbf{e}_z$ is the position of the center of the jth sphere and $\mathbf{e}_z$ is the unit vector along the array. Scattered electromagnetic fields are expanded in a series over vector spherical harmonics $\mathbf{M}_n^m$ and $\mathbf{N}_n^m$ [32,33]

$$\mathbf{E}(\mathbf{r}) = \sum_j e^{i\beta \mathbf{R}_j} \sum_{lm} \left[a_l^m \mathbf{M}_l^m(\mathbf{r} - \mathbf{R}_j) + b_l^m \mathbf{N}_l^m(\mathbf{r} - \mathbf{R}_j) \right],$$

$$\mathbf{H}(\mathbf{r}) = -i \sum_j e^{i\beta \mathbf{R}_j} \sum_{lm} \left[a_l^m \mathbf{N}_l^m(\mathbf{r} - \mathbf{R}_j) + b_l^m \mathbf{M}_l^m(\mathbf{r} - \mathbf{R}_j) \right].$$

$$(1)$$

Here the first (second) terms presents TE (TM) spherical vector EM fields.

In absence of an incident wave Linton *et al.* [32] derived the homogeneous matrix equation for the amplitudes a_l^m, b_l^m

$$Z_{TE,l}^{-1}a_l^m - \sum_\nu \left(a_\nu^m \mathcal{A}_{\nu l}^{mm} + b_\nu^m \mathcal{B}_{\nu l}^{mm} \right) = 0,$$
$$Z_{TM,l}^{-1}b_l^m - \sum_\nu \left(a_\nu^m \mathcal{B}_{\nu l}^{mm} + b_\nu^m \mathcal{A}_{\nu l}^{mm} \right) = 0, \quad (2)$$
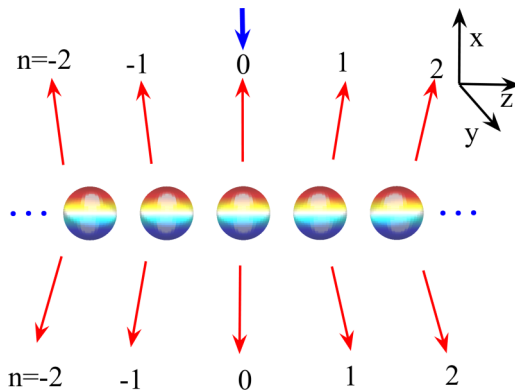

FIG. 1. Periodic infinite array of dielectric spheres with radius R and the dielectric constant ϵ illuminated by a plane wave (blue arrow). The wave can be reflected to discrete diffraction continua given by Eq. (11) and shown by red arrows.

where summation over ν begins with $\max(1,m)$, and $Z_{TE,l}$ and $Z_{TM,l}$ are the so-called Lorenz-Mie coefficients found in Stratton's book [33]. Mathematical expressions of matrix elements $\mathcal{A}_{l\nu}^{mm}$ and $\mathcal{B}_{l\nu}^{mm}$ are rather cumbersome. The reader can find explicit expressions for them in Ref. [32].

The next step is to account for incident plane wave, which can be expanded over vector spherical harmonics [33]:

$$\mathbf{E}^\sigma(\mathbf{r}) = \sum_{l=1}^\infty \sum_{-l}^l \left[q_{lm}^\sigma \mathbf{M}_l^m(\mathbf{r}) + p_{lm}^\sigma \mathbf{N}_l^m(\mathbf{r}) \right],$$

$$\mathbf{H}^\sigma(\mathbf{r}) = -i \sum_{lm} \left[p_{lm}^\sigma \mathbf{M}_l^m(\mathbf{r}) + q_{lm}^\sigma \mathbf{N}_l^m(\mathbf{r}) \right]. \quad (3)$$

Here index σ stands for plane TE or TM wave.

$$p_{lm}^{TE} = -F_{lm}\tau_{lm}(\alpha), \quad q_{lm}^{TE} = F_{lm}\pi_{lm}(\alpha),$$
$$p_{lm}^{TM} = -iF_{lm}\pi_{lm}(\alpha), \quad q_{lm}^{TM} = iF_{lm}\tau_{lm}(\alpha), \quad (4)$$

$$k_x = -k_0 \sin\alpha, \quad k_y = 0, \quad k_z = \beta = k_0 \cos\alpha,$$

$$F_{lm} = (-1)^m i^l \sqrt{\frac{4\pi(2l+1)(l-m)!}{(l+m)!}},$$

$$\tau_{lm}(\alpha) = \frac{m}{\sin\alpha} P_l^m(\cos\alpha),$$

$$\pi_{lm}(\alpha) = -\frac{d}{d\alpha} P_l^m(\cos\alpha). \quad (5)$$

The general equation for the amplitudes a_l^m, b_l^m which describe the scattering by a linear array of spheres takes the following form

$$Z_{TE,l}^{-1}a_l^m - \sum_\nu \left(a_\nu^m \mathcal{A}_{\nu l}^{mm} + b_\nu^m \mathcal{B}_{\nu l}^{mm} \right) = q_{lm}^\sigma,$$

$$Z_{TM,l}^{-1}b_l^m - \sum_\nu \left(a_\nu^m \mathcal{B}_{\nu l}^{mm} + b_\nu^m \mathcal{A}_{\nu l}^{mm} \right) = p_{lm}^\sigma. \quad (6)$$

Thanks to the axial symmetry of the array we can exploit the vector cylindrical modes for description of the diffraction continua which are doubly degenerate in TM and TE polarizations σ. The modes can be expressed through a scalar function ψ [33]

$$\psi_{m,n}(r,\phi,z) = H_m^{(1)}(\chi_n r)e^{im\phi + ik_{z,n}z}. \quad (7)$$

Then for the TE modes we have

$$E_z = 0, \quad H_z = \psi_{m,n},$$

$$E_r = \frac{ik_0}{\chi_n^2}\frac{1}{r}\frac{\partial \psi_{m,n}}{\partial \phi}, \quad H_r = \frac{ik_z}{\chi_n^2}\frac{\partial \psi_{m,n}}{\partial r}, \quad (8)$$

$$E_\phi = \frac{-ik_0}{\chi_n^2}\frac{\partial \psi_{m,n}}{\partial r}, \quad H_\phi = \frac{ik_z}{\chi_n^2}\frac{1}{r}\frac{\partial \psi_{m,n}}{\partial \phi},$$

and for the TM modes

$$E_z = \psi_{m,n}, \quad H_z = 0,$$

$$E_r = \frac{ik_z}{\chi_n^2}\frac{\partial \psi_{m,n}}{\partial r}, \quad H_r = \frac{-ik_0}{\chi_n^2}\frac{1}{r}\frac{\partial \psi_{m,n}}{\partial \phi}, \quad (9)$$

$$E_\phi = \frac{ik_z}{\chi_n^2}\frac{1}{r}\frac{\partial \psi_{m,n}}{\partial \phi}, \quad H_\phi = \frac{ik_0}{\chi_n^2}\frac{\partial \psi_{m,n}}{\partial r},$$

where

$$\chi_n^2 = k_0^2 - k_{z,n}^2 \tag{10}$$

and

$$k_{z,n} = \beta + 2\pi n, \ n = 0, \pm 1, \pm 2, \dots. \tag{11}$$

Therefore the diffraction continua are specified by two quantum numbers m and n where the m is the result of the axial symmetry and n is the result of translational symmetry of the infinite linear array of the dielectric spheres. Note that each diffraction continuum is doubly degenerate relative to the polarization σ. As a result of the interplay between the frequency k_0 and the wave number $k_{z,n}$ the continua can be open (χ is real) or closed (χ is imaginary). In what follows we consider the BSCs embedded into the first radiation continuum $n = 0$ and below the others with $|n| > 0$. Therefore $\beta = k_{z,0}$.

III. EMERGENCE OF THE BSC IN SCATTERING

Let us rewrite Eq. (6) in a compact form [29],

$$\widehat{L}\Psi = \Psi_{\text{inc}}, \tag{12}$$

where the matrix $\widehat{L}$ is defined by the Lorenz-Mie coefficients and matrix elements $\mathcal{A}_{l\nu}^{mm}$ and $\mathcal{B}_{l\nu}^{mm}$, Ψ_{inc} is given by the incident wave and consists of amplitudes q_{lm}^σ and p_{lm}^σ, and the column Ψ consists of amplitudes a_l^m and b_l^m of the multipole expansion of the scattering function. The scattering function can be expressed via the inverse of the matrix $\widehat{L}$,

$$\Psi = \widehat{L}^{-1}\Psi_{\text{inc}}. \tag{13}$$

This equation is a Green's equation in which the source presented by incident plane wave Ψ_{inc} unambiguously gives the solution as the scattered wave Ψ. However, there can be an exception when the inverse of the matrix $\widehat{L}$ does not exist. That occurs if one of complex eigenvalues of $\widehat{L}$ turns to zero:

$$\widehat{L}\Psi_{BSC} = 0. \tag{14}$$

According to the above equation the BSC is a null eigenvector of matrix $\widehat{L}$ with zero eigenvalue. As soon as one deviates from the BSC point in the parametric space the BSC emerges in the form of a collapsing Fano resonance. That phenomenon was observed in scattering of EM waves by arrays of rods [14–16,18,19,21,25]. The Fano resonance for the present system can be interpreted as interference of two optical paths, one through the spheres and another between the spheres. In what follows we highlight these features of the BSCs using the biorthogonal basis of eigenvectors of the non-Hermitian matrix $\widehat{L}$ [15,34]:

$$\widehat{L}\mathbf{X}_f = L_f\mathbf{X}_f, \quad \widehat{L}^+\mathbf{Y}_f = L_f^*\mathbf{Y}_f, \quad \mathbf{Y}_f^+\mathbf{X}_{f'} = \delta_{ff'}. \tag{15}$$

It immediately follows that

$$\widehat{L}^{-1} = \sum_f \mathbf{X}_f \frac{1}{L_f} \mathbf{Y}_f^+. \tag{16}$$

Because of the axial symmetry matrix $\widehat{L}$ has OAM-preserving block structure

$$L_{ll'}^{(m)} = \begin{pmatrix} Z_{TE,l}^{-1}\delta_{ll'} - \mathcal{A}_{ll'}^{mm} & -\mathcal{B}_{ll'}^{mm} \\ -\mathcal{B}_{ll'}^{mm} & Z_{TM,l}^{-1}\delta_{ll'} - \mathcal{A}_{ll'}^{mm} \end{pmatrix}, \tag{17}$$

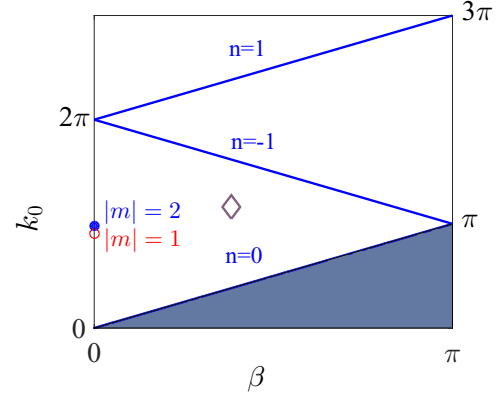where each block corresponds to a specific value m.

FIG. 2. Two BSCs with OAM are marked by closed circles and Bloch BSC with $\beta \neq 0$, $m = 0$ is marked by a rhombus. All BSC points are calculated for spheres with $\epsilon = 15$ [29]. Dashed and dash-dotted lines show thresholds where the next continua $n = \pm 1$ are opened.

In the nearest vicinity of the BSC point one of the complex eigenvalues L_c is close to zero. That allows us to substantially simplify Eq. (16), leaving in the sum only the leading contribution related to L_c. Respectively the scattering function in Eq. (13) is simplified as follows:

$$\Psi^\sigma \approx \frac{1}{L_c}\mathbf{X}_c\left(\mathbf{Y}_c^+ \cdot \Psi_{\text{inc}}^\sigma\right), \quad \sigma = TE/TM. \tag{18}$$

This equation manifests one property that is remarkable as well as important for applications: The BSCs enormously enhance the incident wave Ψ_{inc} by the factor $1/L_c$ [25,30,31]. First this effect for scattering by the infinite periodic array of dielectric spheres was shown in Ref. [29] in the vicinity to the symmetry protected BSCs with $m = 0$. The Bloch BSC with $m = 0$, $\beta \neq 0$ and BSCs with OAM $m \neq 0$, $\beta = 0$ were also found in Ref. [29]. These BSCs exist above the first diffraction continuum $n = 0$ but below the diffraction continuum $n = \mp 1$ as shown in Fig. 2. The BSCs marked by rhombus and closed circles in Fig. 2 are of special interest because in scattering of plane waves in the vicinity of the BSC points they are able to support giant power currents: laminar currents along the array of spheres in the case of the Bloch BSC and vortical currents around the array in the case of BSCs with OAM.

IV. SCATTERING OF PLANE WAVES IN THE VICINITY OF THE BLOCH BSC

In this section we consider the Bloch BSC whose field configuration was obtained in Ref. [29] and shown in Fig. 3. Since the Bloch number $\beta_c = 1.2074$, the EM field configuration is incommensurate with the period of the array, and the EM field is different at each sphere.

The numerical results are presented in Fig. 4(a), which shows that under illumination of the array by a TE plane wave there is a resonant peak only in the total cross section $\sigma_{TE,TE}$ [29]. If a plane wave with TE polarization, the wave vector $(k_x, 0, \beta \approx \beta_c)$, and the frequency $k_0 = k_{0c} = 3.6505$ illuminates the array, the running Bloch quasi-BSC with β is excited as shown in Fig. 4(b). As shown in Fig. 4(b) such a plane wave gives rise to giant laminar power flows.
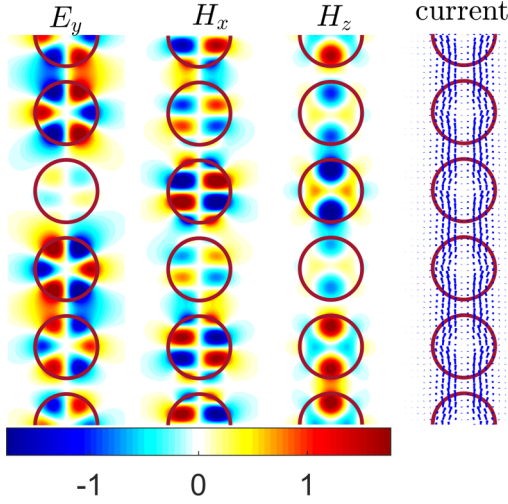
FIG. 3. EM field configurations from Ref. [29] and power current of the Bloch BSC with $\beta_c = 1.2074$, $k_{0c} = 3.6505$, $R_c = 0.4$, $\epsilon = 15$.

V. TRANSFER OF SAM INTO OAM OF THE BSC WITH $m \neq 0$

Scattering of circularly polarized plane waves in the vicinity of the BSCs with OAM is the main issue of this section. Because of the time-reversal symmetry, BSCs with OAM are degenerate with respect to the sgn of m. That modifies Eq. (18) as follows:

$$\Psi_\sigma^m \approx \frac{1}{L_c} \sum_\pm \left[\mathbf{X}_c(\pm m) \left(\mathbf{Y}_c(\pm m)^+ \cdot \Psi_{\text{inc}}^{\pm m, \sigma} \right) \right], \quad (19)$$

where the incident wave according to Eq. (6) is given as

$$\Psi_{\text{inc}}^{m,\sigma} = \begin{pmatrix} \text{sgn}(m)\mathbf{p}_{|m|}^\sigma \\ \mathbf{q}_{|m|}^\sigma \end{pmatrix}, \, m \text{ are odd}, \, \sigma = TE,$$

$$\Psi_{\text{inc}}^{m,\sigma} = \begin{pmatrix} \mathbf{p}_{|m|}^\sigma \\ \text{sgn}(m)\mathbf{q}_{|m|}^\sigma \end{pmatrix}, \, m \text{ are odd}, \, \sigma = TM,$$

$$\Psi_{\text{inc}}^{m,\sigma} = \begin{pmatrix} \mathbf{p}_{|m|}^\sigma \\ \text{sgn}(m)\mathbf{q}_{|m|}^\sigma \end{pmatrix}, \, m \text{ are even}, \, \sigma = TE,$$

$$\Psi_{\text{inc}}^{m,\sigma} = \begin{pmatrix} \text{sgn}(m)\mathbf{p}_{|m|}^\sigma \\ \mathbf{q}_{|m|}^\sigma \end{pmatrix}, \, m \text{ are even}, \, \sigma = TM. \quad (20)$$

and subvectors $\mathbf{p}^m$ and $\mathbf{q}^m$ are given by Eq. (4). In particular, for the plane wave incident normally to the array $\beta = 0$ we have

$$\mathbf{p}_{|m|}^{TE} = \begin{pmatrix} 0 \\ p_{m,2}^{TE} \\ 0 \\ p_{m,4}^{TE} \\ \vdots \end{pmatrix}, \quad \mathbf{q}_{|m|}^{TE} = \begin{pmatrix} q_{m,1}^{TE} \\ 0 \\ q_{m,3}^{TE} \\ 0 \\ \vdots \end{pmatrix}, \quad m \text{ are odd},$$

$$\mathbf{p}_{|m|}^{TM} = \begin{pmatrix} p_{m,1}^{TM} \\ 0 \\ p_{m,3}^{TM} \\ 0 \\ \vdots \end{pmatrix}, \quad \mathbf{q}_{|m|}^{TM} = \begin{pmatrix} 0 \\ q_{m,2}^{TM} \\ 0 \\ q_{m,4}^{TM} \\ \vdots \end{pmatrix}, \quad m \text{ are odd},$$

$$\mathbf{p}_{|m|}^{TE} = \begin{pmatrix} p_{m,1}^{TE} \\ 0 \\ p_{m,3}^{TE} \\ 0 \\ \vdots \end{pmatrix}, \quad \mathbf{q}_{|m|}^{TE} = \begin{pmatrix} 0 \\ q_{m,2}^{TE} \\ 0 \\ q_{m,4}^{TE} \\ \vdots \end{pmatrix}, \quad m \text{ are even},$$

$$\mathbf{p}_{|m|}^{TM} = \begin{pmatrix} 0 \\ p_{m,2}^{TM} \\ 0 \\ p_{m,4}^{TM} \\ \vdots \end{pmatrix}, \quad \mathbf{q}_{|m|}^{TM} = \begin{pmatrix} q_{m,1}^{TM} \\ 0 \\ q_{m,3}^{TM} \\ 0 \\ \vdots \end{pmatrix}, \quad m \text{ are even}.$$
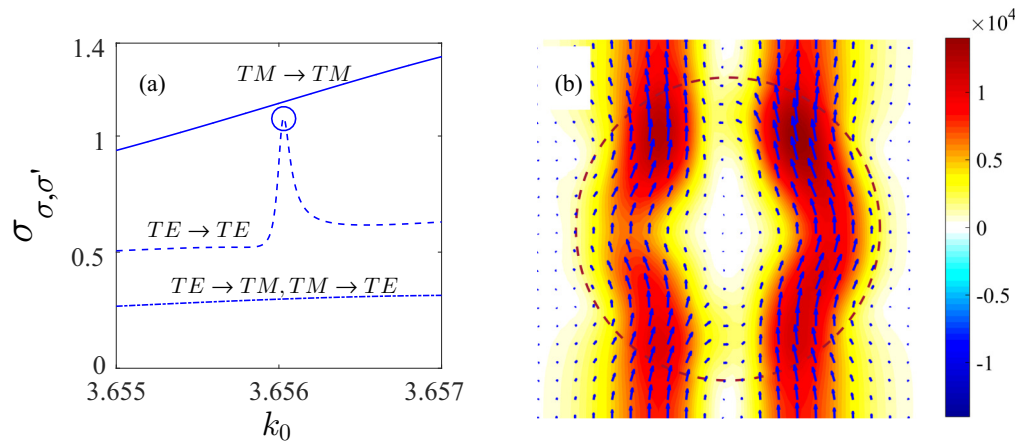
$$(21)$$

FIG. 4. (a) Total cross section for scattering of plane wave with $\beta = 1.3074$ in the vicinity of the Bloch BSC shown in Fig. 3 vs the frequency. (b) The plane wave supports giant laminar power current at the point marked in the left panel by open circle. The color bar at the right indicates absolute value of the current.
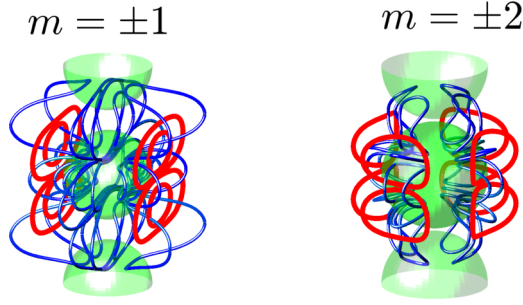
FIG. 5. BSC with orbital angular momentum m. Electric field force lines are shown in red, and magnetic field force lines are shown in blue.

By virtue of Eq. (17) and $\mathcal{B}_{ll'}^{(m)} = -\mathcal{B}_{ll'}^{(-m)}$ the eigenvectors can be decomposed over the polarizations as follows:

$$\mathbf{X}_c(\pm m) = \begin{pmatrix} \mathbf{x}_{TE}^m \\ \pm\mathbf{x}_{TM}^m \end{pmatrix}, \quad \mathbf{Y}_c(\pm m) = \begin{pmatrix} \mathbf{y}_{TE}^m \\ \pm\mathbf{y}_{TM}^m \end{pmatrix}. \tag{22}$$

Then it follows from Eq. (19)

$$\Psi_\sigma^m \approx \begin{cases} \dfrac{D_\sigma^{|m|}}{L_{c,m}}[\mathbf{X}_c(m) + (-1)^m(\mathbf{X}_c(-m)], & \sigma = TE, \\ \dfrac{D_\sigma^{|m|}}{L_{c,m}}[\mathbf{X}_c(m) + (-1)^{m+1}\mathbf{X}_c(-m)], & \sigma = TM, \end{cases} \tag{23}$$

where

$$D_\sigma^{|m|} = \mathbf{y}_{TE}^+\mathbf{p}_{|m|}^\sigma + \mathbf{y}_{TM}^+\mathbf{q}_{|m|}^\sigma. \tag{24}$$

Assume that the elliptically polarized plane wave $\Psi_{\text{inc}}^{TE} + \alpha\Psi_{\text{inc}}^{TM}$ is incident with small β. By taking

$$\alpha = \frac{D_{TE}^{|m|}}{D_{TM}^{|m|}} \tag{25}$$

we obtain from Eq. (23) that

$$\Psi_\sigma \approx F_{|m|}\mathbf{X}_c^{+m}, \quad F_{|m|} = \frac{2D_{TE}^{|m|}}{L_{cm}}. \tag{26}$$

The scattering function has only a contribution with the positive OAM $m > 0$. Here we introduced the enhancement factor F which defines to what extent the scattering function is amplified in the near zone. Respectively for $D_{TE} = -\alpha D_{TM}$ the scattering function has only a contribution with the negative OAM $m < 0$.

Two BSCs with $m = \pm 1$ and $m = \pm 2$ were found in Ref. [29]. The solution for the BSC with $m = 1$ and $\beta_c = 0$ is
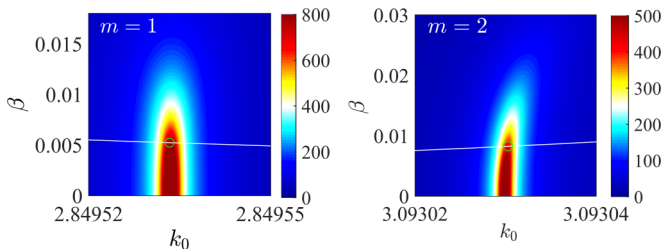

FIG. 6. Enhancement factor $|F_m|$ vs k_0 and β. White line corresponds to polarization (25) $|\alpha| = 1$. Open circles mark maximal enhancement.
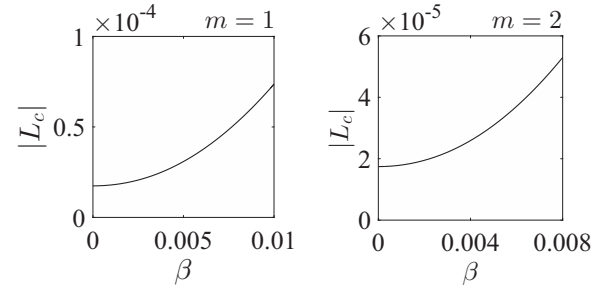

FIG. 7. The lowest eigenvalue $|L_c|$ of matrix (17) in the vicinity of the BSCs with OAM.

the following [29]:

$$\begin{pmatrix} m = 1 \\ l \geqslant 1 \\ k_{0c} = 2.847 \\ R_c = 0.3945 \end{pmatrix},$$

$$(a_l^1, b_l^1) = \begin{pmatrix} 0 & 0.6662 + 0.4273i \\ -0.33 + 0.5145i & 0 \\ 0 & -0.0048 - 0.0031i \\ 0 & 0 \end{pmatrix}. \tag{27}$$

The solution for the BSC with $m = 2$ and $\beta_c = 0$ has the following form:

$$\begin{pmatrix} m = 2 \\ l \geqslant 2 \\ k_{0c} = 3.086 \\ R_c = 0.471 \end{pmatrix},$$

$$(a_l^2, b_l^2) = \begin{pmatrix} 0 & 0.6545 + 0.2013i \\ -0.2142 + 0.6964i & 0 \\ 0 & -0.0057 - 0.0018i \\ 0 & 0 \\ 0 & 0 \end{pmatrix}. \tag{28}$$

These solutions are shown in Fig. 5.

All components of electric and magnetic fields are nonzero and localized around the array as shown in Fig. 5. We show the EM field around only one sphere because the pattern is periodically repeated along the z axis. One can see that the
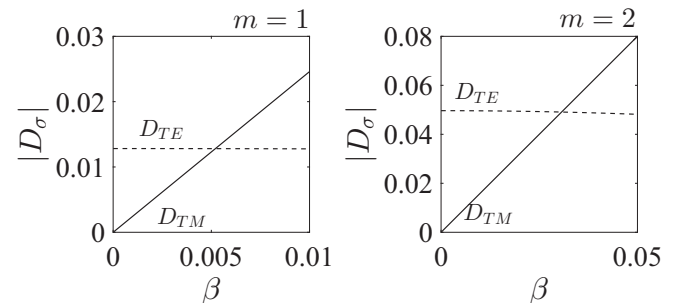

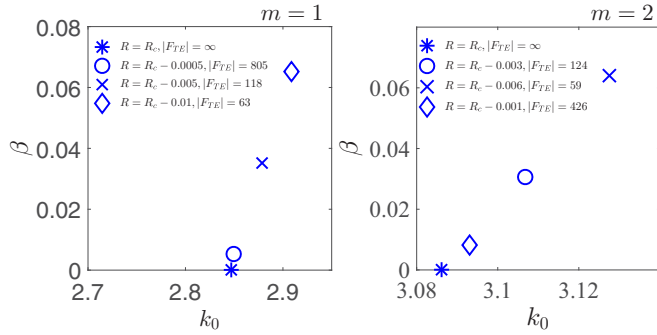FIG. 8. The values D_σ given by Eq. (24) in the vicinity of the BSCs with OAM.

FIG. 9. Values of the maximal enhancement factor $|F|$ vs k_0 and β as dependent on radius of spheres for $|\alpha| = 1$.

FIG. 11. Value of angular component of the power current around the spheres at distance r from the center of sphere and $z = 0$.

value of the azimuthal number m reflects in the structure of force lines in the xy plane while the number of the amplitudes a_l^m reflects in the structure of lines along the z axis.

One can show from Eqs. (21), (27), and (28) that asymptotically $D_{TM}^{|m|} \to 0$ for $\beta \to 0$. From Eq. (26) it follows that the enhancement factor for scattering of plane waves in the vicinity of the BSC point is determined by the ratio D_σ / L_c. In what follows we sweep the frequency of the incident wave k_0 and the angle of incidence defined by β in the vicinity of the BSCs with OAM $m = 1$ and $m = 2$. Figure 6 illustrates the behavior of the enhancement factor in the plane of the frequency k_0 and β calculated with the use of Eq. (26). Following the line with $|\alpha| = 1$ we found the maximal enhancement marked by open green circles in Fig. 6 for the following parameters: (i) For the case of the BSC with $m = 1$ the optimal parameters are $k_0 = k_{0c} + 0.0025$, $\beta = 0.0052$, $\alpha = 0.63 + 0.77i$ for $R = R_c - 0.0005$. (ii) For the case of the BSC with $m = 2$: $k_0 = k_{0c} + 0.02$, $\beta = 0.031$, $\alpha = 0.31 + 0.94i$ for $R = R_c - 0.003$. Fixing these parameters except β we plot the lowest eigenvalue of the matrix $\widehat{L}$ in Fig. 7 and the values of $|D_\sigma|$ Eq. (24) in Fig. 8 versus β. From these figures one can see that, first, the enhancement is determined by the lowest eigenvalue L_{cm} while D_{TE} is almost constant. Second, the value D_{TM} grows from zero. Therefore, to achieve enhancement one has to inject a plane wave with elliptic polarization. In what follows we take for simplicity the circular polarization $|\alpha| = 1$ of the incident wave.

Because of the smallness of the eigenvalue L_{cm} in Eq. (23) EM fields given by the scattering function can reach extremely high values near the spheres. Clearly this is an effect of the BSCs with infinitely high quality factor that presents a possibility to enormously enhance the incident light [16,25,30]. In Fig. 9 we demonstrate that the enhancement is very sensitive to the choice of the sphere radius in the vicinity of R_c when other parameters are tuned to the BSC point.

Thanks to carrying OAM, the BSC with $m \neq 0$ supports vortical power currents [35] as demonstrated in Fig. 10. Owing to the enhancement of the scattered field in the near zone, the spinning currents can reach giant values with respect to the incident power currents as demonstrated in Fig. 11. All currents are measured in terms of the incident power with $\beta = 0.00517$ for the case $m = 1$ and $\beta = 0.0307$ for the case $m = 2$. The value of the current is extremely high inside the spheres but rapidly drops outside the spheres as shown in Fig. 12. As soon as the polarization is linear, for example $\alpha = 0$, vortical currents around the array vanish as demonstrated in Fig. 13.

Figures 14 and 15 demonstrate that the orbital angular momentum of the BSCs affects the scattering of plane waves with linear polarization. The effect is a conversion of the incident polarizations $TE \to TM$ and vise versa. For the normally incident waves $\beta = 0$ there is no polarization conversion and no resonant peaks in the total cross sections $TM \to TM$. Once the angle of incidence deviates from zero $\beta \neq 0$ all three total cross sections acquire resonant response, as shown in Fig. 14. Note that there is polarization conversion when the frequency is far from the BSC frequencies. The absence of polarization conversion is clearly seen in the
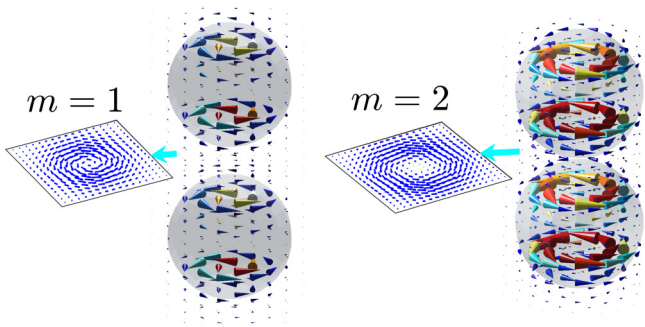

FIG. 10. Pointing current circulates around the spheres when circularly polarized light is injected. Currents around other spheres are repeating periodically.
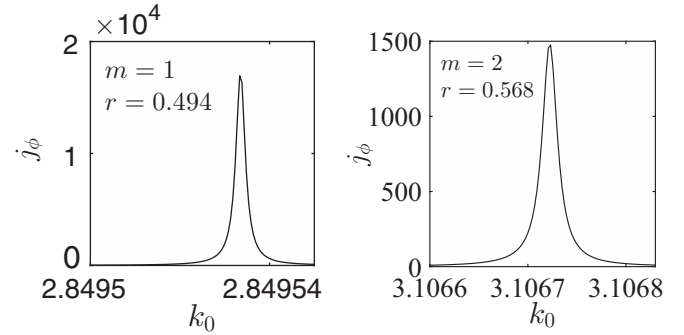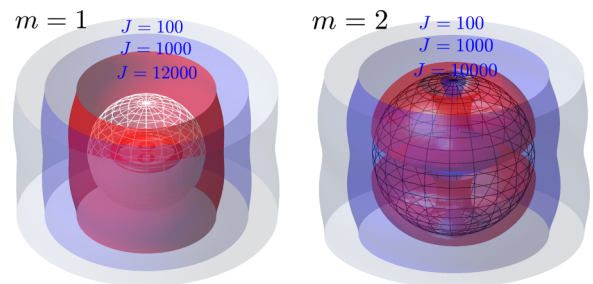

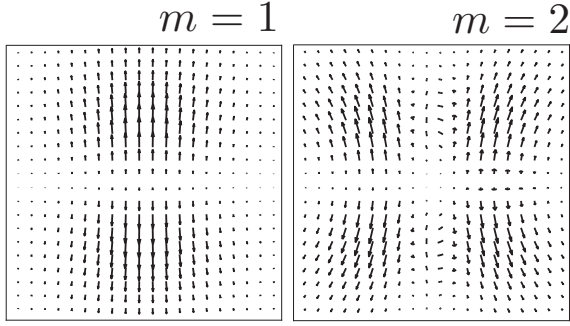FIG. 12. Isosurfaces of constant angular component of the power current.

FIG. 13. Power currents in the middle plane between spheres induced by linearly polarized light with $\alpha = 0$.

differential cross section $TE \to TM$ as shown in Fig. 15. It is also remarkable that this cross section distinctively reflects the value of the OAM m.

VI. DISCUSSIONS AND SUMMARY

As was found in our previous paper [29], the periodical array of dielectric spheres can trap light above the light cone in a variety of the BSCs, the majority of which are symmetry-protected BSCs of both polarizations. Alongside BSCs with OAM, $m = \pm 1$ and $m = \pm 2$ were predicted due to the axial symmetry of the array. These BSCs emerge in the response of the array to incident plane waves with circular polarization. A transfer of the SAM of the incident plane wave into the OAM of EM field takes place for any frequency and wave vector of the incident wave as shown in Fig. 6. The transfer results in the power current spinning around the array. The most remarkable is that as seen from Figs. 6 and 9 in the nearest vicinity of the BSCs with $m \neq 0$ the array supports giant vortical power currents, which are directly related to the extremal enhancement of the scattered field. The value of the current is also sensitive to the distance from the array. It rapidly goes down away from spheres as shown in Fig. 12.

Theoretically the value of the circulating currents can grow up to infinity in the BSC point. However, there are two differences between the present theory and possible experimental realization of the transfer of SAM into OAM, that is, (1) a finite number of the spheres and (2) there are always some losses when the waves transport through the sample

FIG. 15. Differential cross section for scattering of plane wave illuminating the array in the vicinity of the BSC with OAM.

because of material for spheres. The most profound effect of finite arrays is that the BSCs become quasi-BSCs because, unlike a plasmonic sphere, finite dielectric systems cannot support BSCs [26–28]. Therefore, the effect of giant vortical currents around the array can be suppressed. It is believed that for a sufficiently large number of the spheres the lifetime of the quasi-BSC tends to infinity. Below we show numerically that one hundred spheres is quite enough to reach the theoretical limit for giant currents established in the previous section.

For finite number of the spheres the translational invariance is broken. Then Eq. (1) can be modified as follows [32]:

$$\mathbf{E}(\mathbf{r}) = \sum_{j=1}^{N} \sum_{lm} \left[a_j^{lm} \mathbf{M}_l^m(\mathbf{r} - \mathbf{R}_j) + b_j^{lm} \mathbf{N}_l^m(\mathbf{r} - \mathbf{R}_j) \right],$$

$$\mathbf{H}(\mathbf{r}) = -i \sum_{j=1}^{N} \sum_{lm} \left[a_j^{lm} \mathbf{N}_l^m(\mathbf{r} - \mathbf{R}_j) + b_j^{lm} \mathbf{M}_l^m(\mathbf{r} - \mathbf{R}_j) \right].$$

(29)

The expansion coefficients a_j^{lm}, b_j^{lm} were found numerically [36] and presented in Fig. 16. At the first sight it seems that for growing N the solution for amplitudes a_j and b_j should saturate except in the vicinity of the edges of the finite array. However, the EM field is a massless field which has no characteristic scale. Hence we have the behavior of the amplitudes as shown in Fig. 16. Nevertheless we can see a tendency for saturation of the amplitudes to the maximal value with the growth of N, but we always observe non-negligible
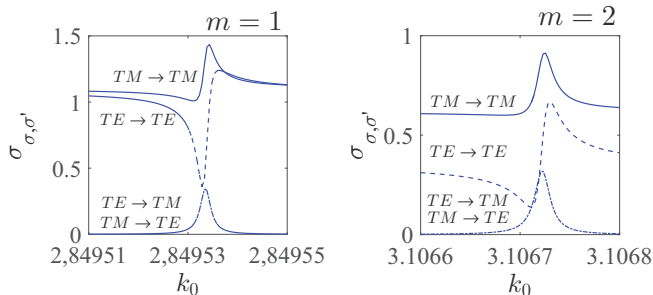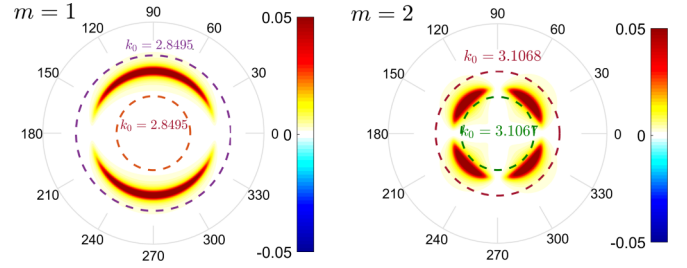

FIG. 14. Total cross section for scattering of plane wave by the array in the vicinity of the BSC with OAM at $\beta = 0.0052$ (left panel) and $\beta = 0.031$.
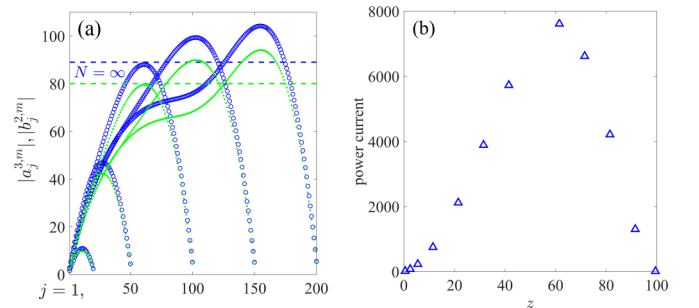

FIG. 16. (a) Values of coefficients a_j^{lm} in Eq. (29) and (b) values of power current at $z = n + 0.5$, $r = 0.25$ where the current is maximal for different number of spheres with $R = 0.468$ for $k_0 = 3.10705$, $k_z = 0.0307$, $\alpha = -0.31 + 0.95i$.

effect of the edges of the finite array. That affects the transfer of SAM of incident light into the giant vortical currents in the vicinity of a quasi-BSC. A similar effect which transforms the BSCs into quasi-BSCs is the volatility of the material parameters of the spheres.

The next problem which can seriously damage the effect of giant spinning currents is the complex dielectric permittivity $\epsilon = \epsilon' + i\epsilon''$. Fortunately, for silicon dielectric particles there is a wide frequency window in the nearest infrared range where the ϵ'' is extremely small [37]. The advantage of dielectric structures is a wide range of BSC wavelengths from microns (photonics) to centimeter (microwave range) as dependent on

the choice of the radius of spheres. Losses when the waves transport through the array result in the finite free path length $L = v_g/\epsilon''\omega$, where v_g is the group velocity. Therefore, it is sufficient to take the number of spheres not exceeding L/h, where h is the period of the array. A particular case of this problem was considered in Ref. [38].

ACKNOWLEDGMENTS

[1] L. Allen, M. W. Beijersbergen, R. J. C. Spreeuw, and J. P. Woerdman, Orbital angular momentum of light and the transformation of Laguerre-Gaussian laser modes, Phys. Rev. A **45**, 8185 (1992).

[2] L. Allen and M. J. Padgett, The Poynting vector in Laguerre-Gaussian beams and the interpretation of their angular momentum density, Opt. Commun. **184**, 67 (2010).

[3] A. M. Yao and M. J. Padgett, Orbital angular momentum: Origins, behavior, and applications, Adv. Opt. Photon. **3**, 161 (2011).

[4] R. Čelechovský and Z. Bouchal, Optical implementation of the vortex information channel, New J. Phys. **9**, 328 (2007).

[5] Yu. Gorodetski, A. Drezet, C. Genet, and T. W. Ebbesen, Generating Far-Field Orbital Angular Momenta from Near-Field Optical Chirality, Phys. Rev. Lett. **110**, 203906 (2013).

[6] H. Yu, H. Zhang, Y. Wang, S. Han, H. Yang, X. Xu, Z. Wang, V. Petrov, and J. Wang, Optical orbital angular momentum conservation during the transfer process from plasmonic vortex lens to light, Sci. Rep. **3**, 3191 (2013).

[7] M. Berezin, E. O. Kamenetskii, and R. Shavit, Topological magnetoelectric effects in microwave far-field radiation, J. Appl. Phys. **120**, 033104 (2016).

[8] A. Zukauskas, M. Malinauskas, and E. Brasselet, Monolithic generators of pseudo-nondiffracting optical vortex beams at the microscale, Appl. Phys. Lett. **103**, 181122 (2013).

[9] R. Dall, M. D. Fraser, A. S. Desyatnikov, G. Li, S. Brodbeck, M. Kamp, C. Schneider, S. Höfling, and E. A. Ostrovskaya, Creation of Orbital Angular Momentum States With Chiral Polaritonic Lenses, Phys. Rev. Lett. **113**, 200404 (2014).

[10] N. Yu and F. Capasso, Optics with designer metasurfaces, Nat. Mater. **13**, 139, (2014).

[11] M. Schäferling, X. Yin, and H. Giessen, Formation of chiral fields in a symmetric environment, Opt. Express **20**, 26326 (2012).

[12] F. J. Rodriguez-Fortuño, I. Barber-Sanz, D. Puerto, A. Griol, and A. Martinez, Resolving light handedness with an on-chip silicon microdisk, ACS Photon. **1**, 762 (2014).

[13] S. P. Shipman and S. Venakides, Resonant transmission near nonrobust periodic slab modes, Phys. Rev. E **71**, 026611 (2005).

[14] R. F. Ndangali and S. V. Shabanov, Electromagnetic bound states in the radiation continuum for periodic double arrays of subwavelength dielectric cylinders, J. Math. Phys. **51**, 102901 (2010).

[15] E. N. Bulgakov and A. F. Sadreev, Bloch bound states in the radiation continuum in a periodic array of dielectric rods, Phys. Rev. A **90**, 053801 (2014).

[16] M. Song, H. Yu, C. Wang, N. Yao, M. Pu, J. Luo, Z. Zhang, and X. Luo, Sharp Fano resonance induced by a single layer of nanorods with perturbed periodicity, Opt. Express **23**, 2895 (2015).

[17] Z. Hu and Y. Y. Lu, Standing waves on two-dimensional periodic dielectric waveguides, J. Opt. **17**, 065601 (2015).

[18] L. J. Yuan and Y. Y. Lu, Nonlinear standing waves on a periodic array of circular cylinders, Opt. Express **23**, 20636 (2015).

[19] C. W. Hsu, B. Zhen, S.-L. Chua, S. G. Johnson, J. D. Joannopoulos, and M. Soljačić, Bloch surface eigenstates within the radiation continuum, Light Sci. Appl. **2**, e84 (2013).

[20] Y. Yang, C. Peng, Y. Liang, Z. Li, and S. Noda, Analytical Perspective for Bound States in the Continuum in Photonic Crystal Slabs, Phys. Rev. Lett. **113**, 037401 (2014).

[21] B. Zhen, C. W. Hsu, L. Lu, A. D. Stone, and M. Soljačić, Topological Nature of Optical Bound States in the Continuum, Phys. Rev. Lett. **113**, 257401 (2014).

[22] L. S. Li and H. Yin, Bound states in the continuum in double layer structures, Sci. Rep. **6**, 26988 (2016).

[23] Z. Wang, H. Zhang, L. Ni, W. Hu, and C. Peng, Analytical perspective of interfering resonances in high-index-contrast periodic photonic structures, IEEE J. Quantum Electron. **52**, 6100109 (2016).

[24] X. Gao, C. W. Hsu, B. Zhen, X. Lin, J. D. Joannopoulos, M. Soljačić, and H. Chen, Formation mechanism of guided resonances and bound states in the continuum in photonic crystal slabs, Sci. Rep. **6**, 31908 (2016).

[25] M. Zhang and X. Zhang, Ultrasensitive optical absorption in graphene based on bound states in the continuum, Sci. Rep. **5**, 8266 (2015).

[26] M. G. Silveirinha, Trapping light in open plasmonic nanostructures, Phys. Rev. A **89**, 023813 (2014).

[27] F. Monticone and A. Alu, Embedded Photonic Eigenvalues in 3D Nanostructures, Phys. Rev. Lett. **112**, 213903 (2014).

[28] I. Hrebikova, L. Jelinek, and M. G. Silveirinha, Embedded energy state in an open semiconductor heterostructure, Phys. Rev. B **92**, 155303 (2015).

[29] E. N. Bulgakov and A. F. Sadreev, Light trapping above the light cone in one-dimensional array of dielectric spheres, Phys. Rev. A **92**, 023816, (2015).

[30] A. F. Sadreev, E. N. Bulgakov, and I. Rotter, Bound states in the continuum in open quantum billiards with a variable shape, Phys. Rev. B **73**, 235342 (2006).

[31] E. N. Bulgakov, K. N. Pichugin, A. F. Sadreev, and I. Rotter, Bound states in the continuum in open Aharonov—Bohm rings, JETP Lett. **84**, 430 (2006).

[32] C. M. Linton, V. Zalipaev, and I. Thompson, Electromagnetic guided waves on linear arrays of spheres, Wave Motion **50**, 29 (2013).

[33] J. A. Stratton, *Electromagnetic Theory* (McGraw-Hill, New York, 1941).

[34] A. F. Sadreev and I. Rotter, *S*-matrix theory for transmission through billiards in tight-binding approach, J. Phys. A **36**, 11413 (2003).

[35] E. N. Bulgakov and A. F. Sadreev, Giant optical vortex in photonic crystal waveguide with nonlinear optical cavity, Phys. Rev. B **85**, 165305 (2012).

[36] Y.-L. Xu, Electromagnetic scattering by an aggregate of spheres: Far field, Appl. Optics **36**, 9496 (1997).

[37] M. A. Green and M. J. Keevers, Optical properties of intrinsic silicon at 300 K, Progr. Photovoltaics. **3**, 189 (1995).

[38] E. N. Bulgakov and D. N. Maksimov, Light guiding above the light line in arrays of dielectric nanospheres, Opt. Lett. **41**, 3888 (2016).